Analysis and Research of High Voltage Cable Head Insulation Discharge Diagnosis Based on Various Detection Methods

Yang Zhao[1]*, **Qing Liu**[1], **Tong Shang**[1], **Yingqiang Shang**[1], **Rong Xia**[2], **Shuai Shao**[3]

[1] *State Grid Beijing Powercable Company, Beijing 100022, China*
[2] *China Electric Power Research Institute Limited Wuhan Branch, Wuhan 430079, China*
[3] *Center of Jinan Power Supply Company of State Grid Shandong Electric Power Company, Jinan 250012, China*

Because there are many and complex types of high-voltage cable head insulation discharge, the accuracy of the discharge diagnosis decreases and the diagnosis time increases. Therefore, a new method for diagnosing high-voltage cable head insulation discharge based on multiple detection methods is proposed and tested. The proposed method involves using the fiber Bragg grating to collect the insulation discharge acoustic signal of high voltage cable head, and using subspace reconstruction, frequency slicing wavelet and fast independent component analysis to suppress interferences due to periodic narrow-band, white noise, and random impulse. The M-ary support vector machine is used to classify the insulation discharge signals of a high-voltage cable head, and achieve the discharge diagnosis. The experimental results show that for the four types of typical high-voltage cable head insulation discharges (needle plate discharge, internall discharge, suspension discharge and surface discharge), the proposed method achieves a high level of diagnostic accuracy and the diagnosis time is short. Hence, the proposed method can achieve rapid and accurate diagnosis of high-voltage cable head insulation discharge.

Keywords: high-voltage cable head; insulation discharge diagnosis; fiber Bragg grating; subspace reconstruction; frequency slice wavelet; fast independent component analysis; M-ary support vector machine

1. INTRODUCTION

Sustainable industrial development requires higher power quality to ensure the stability of the power supply, and the power supply quality is directly related to the power equipment adopted [1]. Measures must be taken to ensure that all power equipment is in a stable working state, faults or potential safety hazards are discovered in a timely manner, and effective steps must be taken to prevent interference with the normal operation of the power equipment. With the continuous improvement of China's existing power industry installation capacity and total power generation, the demand

for power transmission equipment is increasing rapidly, and the application scenarios of cable technology will gradually expand. Studies in this field continue to increase, and many new products and technologies have been adopted by various industries [2]. On the one hand, with the increasing development of China's urban modernization, land resources are becoming more and more precious. The power cable transmission system is widely used in many cities because it saves land resources and does not affect the landscape. On the other hand, although wind power and photovoltaic power generation are becoming the new sources of power generation and the focus of the development of new energy technology, the power cable is less susceptible to changes in the external environment, effectively improves the security of the collector

---

*Email of corresponding author: zhaoyang@mjc-edu.cn
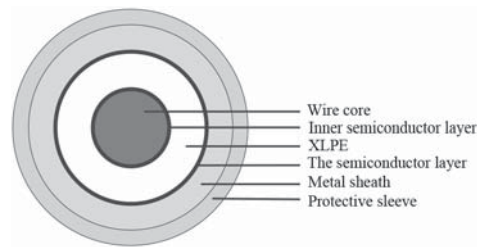
Figure 1 Body structure of 10kV XLPE cable.

system and the stability of power system transmission, and is therefore favored by power-generation enterprises [3]. The insulation application technology of the power cable has been developing for a hundred years. With the improvement of the maximum working voltage and operation stability of the cable, the cable insulation materials have begun to change. Many new materials have shown superior performance in the application, including new materials such as crosslinked polyethylene. However, after the cable is built and put into use, it will be subjected to the effects of electricity, heat and machinery for a long time, and its performance will gradually age and deteriorate. Meanwhile, any minor defects in its manufacturing and construction may further deteriorate with the gradual increase in operation time [4]. Due to the harsh operating environment of cable lines, insulation performance is degraded due to water inflow and dampness in cable trenches, tunnels, pipes and shafts. The section of high-voltage cables is the weak link of cable lines, and the electrical stress at the insulation shielding fracture of cable joints and terminals is relatively concentrated and prone to failure. A cable joint has a closed-end insulation structure and general requirements on site installation is complete. Compared with the ontology and outdoor terminal, insulation small safety margin, high construction quality requirements, such as the construction technology, dustproof measures do not reach the designated position, poor sealing will bury hidden dangers. Therefore, the cable joint became the most prone to cable line insulation fault of vulnerabilities, the failure probability and statistics. The failure rate of cable ends is about 70%, so it is essential to diagnose the insulation discharge of the high-voltage cable end, find the potential defects and risks in time, and establish an appropriate maintenance strategy and operation plan.

Reference [5] proposed an intelligent sensing and monitoring method based on edge computing to determine the state of the cable joint operation. The detection unit developed by [5] was intended to facilitate the observation and analysis of the status of the substation cable joint operation network through the acquisition, data transmission, processing and feature identification of ultraviolet and infrared signals released during the partial discharge process of the cable joint. An adaptive neural fuzzy system (ANFIS) is used to fuse and analyze the two kinds of information to achieve intelligent sensing and diagnosis of cable joint operation status. Reference [6] proposed a distributed optical fiber ultrasonic sensor to detect cable joint discharge faults. Phase-sensitive optical time domain reflectometer is used to study partial discharge in cable joint fault diagnosis. To diagnose discharge, the variations of the Rayleigh scattering coherent light signal can be used to detect the amount of weak ultrasonic

signals. Reference [7] proposed a cable joint partial discharge method based on optical fiber sensing technology. Their design is based on a phase-sensitive optical time-domain reflectometer, distributed optical fiber sensing system with adjacent weak grating optical fiber as the sensing unit, by detecting weak fiber grating adjacent interference signal, can obtain a cable joint between partial discharge acoustic vibration signals, such as frequency, phase and position information, in order to determine the strength of the partial discharge and its location.

Because there are several types of complex high-voltage cable head insulation discharge, the methods proposed by the aforementioned researchers have less accuracy and are more time consuming. Hence, in this paper, a novel method based on multiple detection approaches is proposed for the diagnosis of discharge.

2. DESIGN OF DIAGNOSIS METHOD OF INSULATION DISCHARGE OF HIGH VOLTAGE CABLE HEAD

2.1 Parameters of the Research Object

The focus of this paper is on the main insulation material of 10kV XLPE (cross-linked polyethylene) cable joint (cold shrinkage prefabricated). The main insulation of the body is XLPE and the prefabricated insulation is silicone rubber (SIR). The design defect of the main insulation material is simulated. An XLPE-insulated cable has incomparable advantages over a PVC-insulated cable [8–9], and is widely used for its excellent properties such as simple structure, light weight, good heat resistance, strong load capacity, non-melting, chemical corrosion resistance and high mechanical strength. Figure 1 depicts the structure of the 10kV XLPE cable.

The structure of the high-voltage cable head consists of both prefabricated and integrated prefabricated components. Prefabricated cable components are preferred for high-voltage cables. They are factory-made insulators with pre-fabricated connectors. In recent years, prefabricated cable connectors have been widely used due to their simple structure and convenient installation [10–11]. The main XLPE insulation is connected to the external rubber insulation to maintain the huge pressure of the interface insulation, and requires the outer rubber insulation to have large tension and relaxation capacity, so as to avoid insulation failure caused by damage during the installation process [12]. Also, in the long-term, due to its
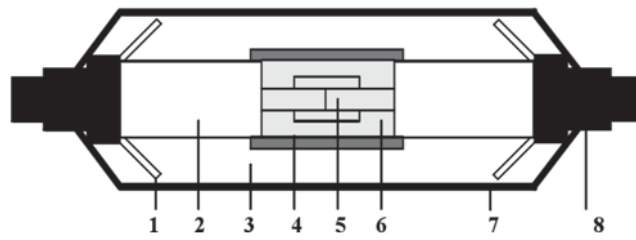
Figure 2 Simple structure of prefabricated joint.

Table 1 Material properties.

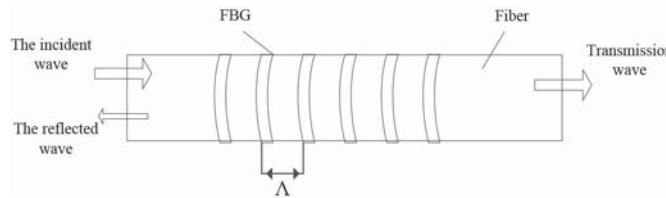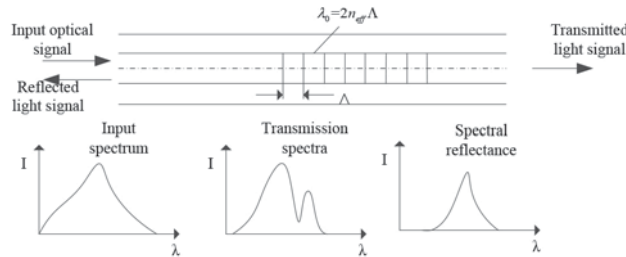| The name of the	Dielectric constant	Thickness of the/mm	Outer diameter/mm
Copper core	–	10	10
Main insulation (XLPE)	2.3	10	20
Connector conduit	100	5	25
Stress cone semiconductor layer	–	5	25
Copper shield	–	5	30
Silicone insulation	3.6	20	40

Figure 3 Fiber grating structure.

Figure 4 Reflection spectrum of fiber grating.

relative elasticity, it will not relax, ensuring a long operating life. The simple structure of the prefabricated joint is shown in Figure 2.

In the figure, 1 is the stress cone semiconductor layer, 2 is the MAIN insulation layer of XLPE, 3 is the rubber insulation layer to enhance the insulation, 4 is the shielding pipe, 5 is the wire core (copper), 6 is the connecting pipe, 7 improves the insulation shielding [13], and 8 is the shielding layer. Several typical defects of XLPE cable joints and their causes and phenomena are described below.

The material parameters and structural parameters required for each part are listed in Table 1, and include the dielectric constant of the material.

2.2 Discharge Acoustic Signal Acquisition Based on Fiber Bragg Grating

Fiber Bragg grating (FBG) is the most widely-used fiber grating. FBG is an optical fiber device with permanent periodic refractive index change in the optical fiber core by some means. The periodic change of its refractive index will have a strong reflection effect on the light of a very narrow bandwidth, and this reflection complies with the Bragg diffraction principle in terms of mechanism, so it is called FBG [14–15]. When an acoustic signal is applied to FBG, it will produce an elastic and optical effect and geometric effect, which will cause the change of refractive index and period, subsequently changing the central wavelength of the grating reflection spectrum. The structure and reflection spectrum of fiber grating are shown in Figure 3 and Figure 4.

When light passes through FBG, the central wavelength λ_0 of FBG reflection spectrum is:

$$\lambda_0 = 2n_{eff}\Lambda$$

Where n_{eff} represents the effective refractive index, and Λ represents the grating period.

When an acoustic emission acts on FBG, strain changes will occur, which will lead to changes in FBG effective refractive index and grating period, and ultimately change the central
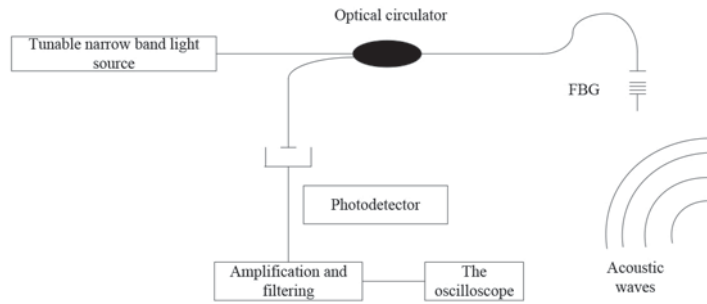
Figure 5 Sound signal acquisition architecture of high voltage cable head insulation discharge based on FBG.

wavelength of FBG reflection spectrum, that is, the change of the central wavelength of FBG reflection spectrum is due to changes in both effective refractive index and grating period [16], so:

$$\lambda_0 = 2(\Delta n_{eff} \cdot + n_{eff} \cdot \Delta \Lambda)$$

$$\frac{\Delta \lambda_0}{\lambda_0} = \frac{\Delta n_{eff}}{n_{eff}} + \frac{\Delta \Lambda}{\Lambda}$$

where Δn_{eff} represents the effective refractive index change, and $\Delta \Lambda$ represents the grating periodic change.

Then the following formula is established:

$$\frac{\Delta n_{eff}}{n_{eff}} = -\frac{n_{eff}^2}{2}[(1 - v) - v P_{11}]\varepsilon(z, t)$$

$$\frac{\Delta \Lambda}{\Lambda} = \varepsilon(z, t)$$

$$\varepsilon(z, t) = \varepsilon_m \cos\left(\frac{2\pi}{\lambda_s}z - w_s t\right), \ z \in [0, L]$$

where v is the Poisson ratio, P_{ij} is elastic-optical coefficient [17–19], λ_s is acoustic emission wavelength, w_s is angular frequency, and ε_m is strain amplitude.

Substituting Formula (4) $\sim$ Formula (6) into Formula (3), can obtain:

$$\Delta \lambda_0 = \lambda_0 \left\{ 1 - \frac{n_{eff}^2}{2}[(1 - v)P_{12} - v P_{11}] \right\} \varepsilon(z, t)$$

$$= \lambda_0 \left\{ 1 - \frac{n_{eff}^2}{2}[(1 - v)P_{12} - v P_{11}] \right\}$$

$$\times \varepsilon_m \cos\left(\frac{2\pi}{\lambda_s}z - w_s t\right)$$

Then the central wavelength of FBG after strain action is named as:

$$\lambda_0' = \lambda_0 + \Delta \lambda_0$$

It can be seen from Formula (7) and Formula (8) that the central wavelength offset of FBG reflects the strain change caused by acoustic signal action of FBG.

Figure 5 shows the acquisition architecture of the insulation discharge sound signal of high-voltage cable head based on FBG.

In this architecture, the tunable narrowband laser can continuously emit narrowband light with different central wavelengths. The narrowband light enters FBG through the optical circulator, and the narrowband light conforming to

Bragg condition is reflected. The narrowband light enters the photodetector through the optical circulator and is converted into an electrical signal that is displayed on an oscilloscope through amplification and filtering.

2.3 Interference Suppression of High Voltage Cable Head Insulation Discharge Sound Signal

The interference of the insulation discharge sound signal of a high-voltage cable head can be periodic narrowband interference, white noise interference, or random pulse interference. The periodic narrowband interference basically comes from the radio signals in the power network and some environmental space. In particular, the narrowband signals which coincide with the frequency of the detection platform will have a great influence on the accuracy of the partial discharge signal measurement. White noise interference is mainly a stationary random signal caused by the thermal noise of electrical equipment. Its power spectral density is uniformly distributed in the frequency domain, and its mathematical expectation and variance are time-independent. Random pulse interference is generally caused by the random interference signals generated when switches, relays and SCR devices are closed or switched off. These interference signals will seriously affect the accuracy of the insulation discharge sound signals obtained from high-voltage cable heads.

2.3.1 Narrowband Interference Suppression Based on Subspace Reconstruction

Subspace reconstruction to suppress narrowband interference involves constructing a HANKEL matrix from the original noisy signal and decomposing it into singular value. From the distribution characteristics of singular value, the partial discharge space and narrowband interference subspace matrix with white noise interference can be separated, and then the narrowband interference can be reconstructed to obtain the partial discharge signal with white noise interference. The HANKEL matrix is constructed as follows:

Assuming that the target signal sequence is F, it can be expressed as:

$$F = \{f(1), \ f(2), \dots, f(N)\}$$

Where N is the total number of sampling points, and HANKEL matrix is constructed from target signal F to obtain:

$$H_{p \times q} = \begin{bmatrix} f(1) & f(2) & \cdots & f(q) \\ f(2) & f(3) & \cdots & f(q+1) \\ \vdots & \vdots & \ddots & \vdots \\ f(p) & f(p+1) & \cdots & f(N) \end{bmatrix}$$

In the formula, satisfy $p + q = N + 1$, the value of q ranges from $\left[\frac{N}{4}, \frac{N}{3} \right]$.

According to the HANKEL matrix obtained, the narrowband interference can be removed and the frequency of narrowband interference can be calculated respectively. Narrowband interference frequency is determined by the matrix beam algorithm, where the target signal is represented by a linear combination of M exponents.

$$f(kT_s) = X(kT_s) + n(kT_s) = \sum_{i=1}^{M} R_i e^{(-\alpha_i + j\omega_i)kT_s} + n(kT_s)$$

where $X(kT_s)$ represents periodic narrowband interference signal, $n(kT_s)$ represents partial discharge signal with white noise interference, R_i is the complex amplitude of periodic narrowband interference, α_i is attenuation parameter, ω_i is angular frequency, M is the order of target partial discharge signal, and T_s is the time interval of oscilloscope sampling. The constructed HANKEL matrix is decomposed according to Formula (12).

$$H = USV^T$$

Based on the decomposition results, the singular values are sorted, and the column vectors of the M larger singular values σ_i in diagonal matrix S are selected to form matrix S_1. The singular phase of the corresponding V consists of $V' = (v_1, v_2, \ldots, v_M)$, V_1 for V', eliminate the first row, V_2 for V', eliminate the last row. Then the following formula holds:

$$\begin{cases} Y_1 = US_1V_1^T \\ Y_2 = US_2V_2^T \end{cases}$$

Assume that the generalized eigenvalue of $Y_2 - \lambda Y_1$ is denoted by z_i, and the narrowband interference frequency can be obtained from Formula (14) to achieve the suppression of interference.

$$f_i = \frac{1}{2\pi} \times \frac{\ln z_i}{T_s}$$

Narrowband interference is removed by the HANKEL matrix, and the first 12 singular values are determined as narrowband interference subspaces according to the size of the singular values, and the rest are combined subspaces of partial discharge and white noise interference. The inverse process of singular value decomposition is narrowband interference signal after denoising.

2.3.2 White Noise Suppression Based on Frequency Slice Wavelet

Frequency slice transform (FSWT) is a new time-frequency analysis method, which has achieved good results in an experimental system used to detect bridge damage. It combines the advantages of STFT and wavelet analysis; the introduced frequency slice function has the symmetry of time domain and frequency domain. The FSWT transformation of the noisy pd signal in the frequency domain can be expressed as:

$$W_F(t, \omega, \delta) = \frac{1}{2\pi} \int_{-\infty}^{\infty} \hat{F}(u) \hat{P} * \left(\frac{u - \omega}{\delta} \right) du$$

where t is the signal moment, w is the frequency value, δ is the scale factor, u is the estimated frequency, $*$ is the conjugate, $\hat{P}$ is the fast Fourier transform result of frequency slice function $P(t)$, and $\hat{F}$ is the fast Fourier transform result of the noisy partial discharge signal. $P(t)$ is selected as:

$$P(t) = \frac{1}{\sqrt{2\pi}} e^{-0.5t^2}$$

Based on the Morlet transformation idea, the scale factor is established, then Formula (16) can be transformed into:

$$W_F(t, \omega, k) = \frac{1}{2\pi} \int_{-\infty}^{\infty} \hat{F}(u) \hat{P} * \left(k \frac{u - \omega}{\delta} \right) e^{int} du$$

Here,

$$k = \frac{\Delta \omega_p}{\eta_s}$$

where k is the dynamic scale that controls the time domain and frequency resolution of FSWT, $\Delta \omega_p$ is the size of frequency window, and η_s is the ratio of time to frequency of noisy signal.

According to the frequency of the noise signal, the white noise interference of the insulation discharge of the high voltage cable head is removed in order to suppress white noise interference.

2.3.3 Random Pulse Interference Suppression Based on Fast Independent Component Analysis

Fast independent component analysis (Fast ICA) can suppress random pulse interference and carry out a fast Fourier transform on noisy signals. After finding frequency spectrum peak, the number of narrowband interferences was determined by information entropy, and each narrowband interference frequency was obtained with the approximation method. According to the information entropy expression, the smaller the power, the smaller is the proportion. Therefore, the information entropy is a bounded value. When the information entropy approaches the bounded value, the number of power values preceding it is the number of narrowband interferences. The expression for information entropy is:

$$H(Y) = -\sum_{i=1}^{n} p_i \lg(p_i)$$

where

$$p_i = \frac{P[peak\_i]}{\sum_{j=1}^{n} P[peak\_j]}$$

$$\sum_{i=1}^{n} p_i = 1$$

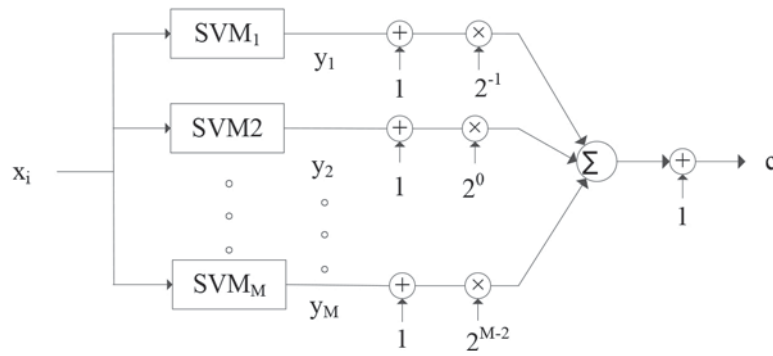and n is the number of extreme values in the frequency spectrum.

Figure 6 Multi-classification support vector machine model based on M-ary.

Finally, six narrowband frequencies are determined, and the values of each narrowband frequency are obtained with the approximation method based on the frequency spectrum.

Random pulse interference manifests as an oscillation pulse, so the first what extracted to determine the length of the data points in all pulses, based on the pulse number of data points, determine the length of the data points. σ_T standard deviation due to the pulse of time domain and frequency domain σ_F is characteristic of the pulse parameters. The standard deviation for each pulse according to Formula (22) and Formula (23) to calculate two important characteristic parameters. Then, the characteristic parameters are clustering by K-means, and finally, the random pulse interference data are compressed to suppress random pulse interference.

The time domain standard deviation σ_T and frequency domain standard deviation σ_F of the pulse can be obtained with:

$$\sigma_T = \sqrt{\frac{\sum_{i=1}^{n}(x_i - \bar{x})^2}{n-1}}$$

$$\sigma_F = \sqrt{\frac{\sum_{j=1}^{n}(X_i - \bar{X})^2}{m-1}}$$

where x represents a single pulse data point, $\bar{x}$ represents the time-domain average value of the pulse, n represents the data points of the pulse. In this paper, 100 is taken, X is the decomposition result of the fast Fourier transform of the pulse, $\bar{X}$ is the average value of the analysis result in the frequency domain, and m is the frequency points.

2.4 High-Voltage Cable Head Insulation Discharge Diagnosis Based on M-ary Support Vector Machine

The M-ary support vector machine is a method proposed by Sebald and Buchlew et al in 2001 to solve the problem of multi-classification of SVM. The method divides multiple category vectors into combinations of multiple binary classification vectors, thus transforming the multi-classification problem into multiple binary classification problems. The number of binary classification classifiers to be constructed is $M =$ $\log_2 k$. k is the total number of categories of problems to be identified. The number of classifiers constructed is less than those obtained with the traditional "one-to-one" and "one-to-many" methods, which reduces the amount of calculation required, improves the classification speed, and improves the efficiency and accuracy of the insulation discharge diagnosis of high-voltage cable heads.

By constructing multiple classifiers, the SVM model based on M-ary divides the total sample into multiple groups and compares any two groups to determine the final category of the sample, in order to solve the multi-classification problem. Assume that all samples of insulation discharge sound signals of the high-voltage cable head are $S = \{x_1, x_2, \ldots, x_k\}$, where x_i is the multi-category samples to be identified, and the number of sub-classifiers required is M. For any m-th sub-classifier, all samples can be divided into two categories, each with a category label. The sample set with category label "+1" is represented by A_m, and the sample set with category label "−1" is represented by B_m.

The m-th classifier divides samples into positive categories. The classification strategy of insulation discharge sound signals of high-voltage cable heads can be expressed as:

$$A_m = \{x_i \in S : \lfloor (x_i - 1) \cdot 2^{-(m-1)} \rfloor\}$$

where the symbol $\lfloor x \rfloor$ represents a downward integer; that is, the value must be the largest integer less than x. Among the total samples, except for those classified as "+1", the remaining samples are labeled as "−1". The classification strategy can be expressed as:

$$B_m = \frac{S}{A_m}$$

The established multi-classification support vector machine model based on M-ary is shown in Figure 6.

In the figure, y_i is the corresponding output category label of the sample under the pattern recognition of each sub-classifier. The final category result c of the sample can be obtained through combination. The judgment is based on Formula (26):

$$c = 1 + \sum_{i=1}^{k} [y_i + 1] \cdot 2^{i-2}$$

This multi-classification SVM classifier model based on M-ary theory also needs to build various sub-classifiers. After determining the computational efficiency and development

history of the support vector machine, the least square support vector mechanism is selected as the sub-classifier to build the classifier.

The LS-SVM algorithm can be derived in the following way to solve the classification problem using optimization method with equality constraints:

$$\begin{cases} \min\limits_{w,b,\xi} J(w,b,\xi) = \frac{1}{2}||w||^2 + \frac{1}{2}C\sum\limits_{i=1}^{N}\xi_i^2 \\ s.t.\ y_i[w\cdot\varphi(x_i)+b] = 1-\xi_i \end{cases}$$

where w represents the weight of the optimal classification hyperplane, b represents the intercept of the optimal classification hyperplane in the coordinate system, ξ represents the classification fault tolerance of the sample, $||w||$ represents the L_2 norm of w, and C represents the weight vector of the sample.

The corresponding Lagrange equation is:

$$L(w,b,\xi,\alpha) = J(w,b,\xi,)-\sum_{i=1}^{N}\alpha_i\{y_i[w\cdot\varphi(x_i)+b]-1+\xi_i\}$$

where α_i is the Lagrange factor, which can be positive or negative because the constraint condition is equality.

According to KKT conditions, the partial derivative of Formula (28) with respect to w and b is obtained, and its partial integral is equal to 0. Then:

$$\begin{cases} \frac{\partial L}{\partial w} = 0, w = \sum\limits_{i=1}^{M}\alpha_i y_i\varphi(x_i) \\ \frac{\partial L}{\partial b} = 0, w = \sum\limits_{i=1}^{M}\alpha_i y_i = 0 \\ \frac{\partial L}{\partial w} = 0 \Rightarrow \alpha_i = C\xi_i \\ \frac{\partial L}{\partial \alpha} = 0, y_i[w^T\varphi(x_i)+b]-1+\xi_i = 0 \end{cases}$$

Formula (29) can be converted into the following equation set:

$$\begin{bmatrix} I & 0 & 0 & -Z^T \\ 0 & 0 & 0 & -Y^T \\ 0 & 0 & C\cdot I & -I \\ Z & Y & I & 0 \end{bmatrix}\begin{bmatrix} w \\ b \\ \xi \\ \alpha \end{bmatrix} = \begin{bmatrix} 0 \\ 0 \\ 0 \\ e \end{bmatrix}$$

where $Z = (\varphi(x_1)^T y_1, \varphi(x_2)^T y_2, \ldots, \varphi(x_N)^T y_N)^T$, $y = (y_1, y_2, \ldots, y_N)^T$, $e = (1, 1, \ldots, 1)^T$, I is the identity matrix, and parameters w and ξ are eliminated. The final calculated result is:

$$\begin{bmatrix} 0 & -Y^T \\ Y & ZZ^T + C^{-1}\cdot I \end{bmatrix}\begin{bmatrix} b \\ \alpha \end{bmatrix} = \begin{bmatrix} 0 \\ e \end{bmatrix}$$

The original optimization problem with equality constraints is transformed into linear equations, and the values of Lagrange factor α and parameter b are obtained. This method is simpler and more efficient than the general quadratic programming approach.

The steps of the M-ary multi-classification LS-SVM algorithm based on the improved DE-PSO for the diagnosis of high voltage cable head insulation discharge are as follows:

Step 1: Classify the characteristic vectors of the insulation discharge sound signals of the high voltage cable ends obtained, and classify the sample category labels according to the defect types of the high-voltage cable ends.

Step 2: Normalize the sample data according to the demand, extract a certain proportion of data sets from the feature vector data set as the training set, and the remainder as the test set;

Step 3: Build a multi-classification LS-SVM model based on M-ary;

Step 4: For each LS-SVM, the improved DE-PSO optimization algorithm is used to search for the regular factor and kernel function parameters of the SVM classifier.

Step 5: Use the training set data to train the MULTI-classification LS-SVM model classifier based on M-ary to optimize its performance;

Step 6: Use test sets to test the performance of the classifier.

Finally, a high-performance high voltage cable head insulation discharge identifier is obtained to achieve the diagnosis of a high-voltage cable head insulation discharge.

3. EXPERIMENTAL DESIGN AND RESULT ANALYSIS

3.1 Experimental Design

In order to determine the effectiveness of the diagnostic method based on multiple detection methods, a simulation test was carried out. In this paper, several typical discharge models designed to simulate the insulation discharge of high voltage cable head are: needle plate discharge, internal discharge, suspension discharge and surface discharge. Their structures are shown in Figure 7.

(1) Needle plate discharge: the radius of curvature of the high-pressure tip is 0.5 mm, the cone angle is 30°, and the tip length is 15 mm. An epoxy resin insulation board with a diameter of 100 mm and a thickness of 1mm is placed on the plate electrode; the distance of the needle plate is 5 mm.

(2) Internal discharge model: the upper and lower layers of the discharge model comprise a 3 mm thick epoxy resin board, and the middle layer is a 1 mm thick epoxy resin board used as the insulation medium. There are round holes with a diameter of 10 mm on the insulation board, and the insulation boards are bonded with epoxy resin glue.

(3) Suspension discharge: the distance between two plate electrodes is 10 mm, the grounding electrode is placed on the diameter of 100 mm, 5 mm thick epoxy resin plate, epoxy resin plate is placed near the edge of 10 mm diameter, 10 mm high copper column;

(4) Discharge along the surface: an epoxy rod with a diameter of 10 mm and a length of 10 mm is placed longitudinally between the two plate electrodes.
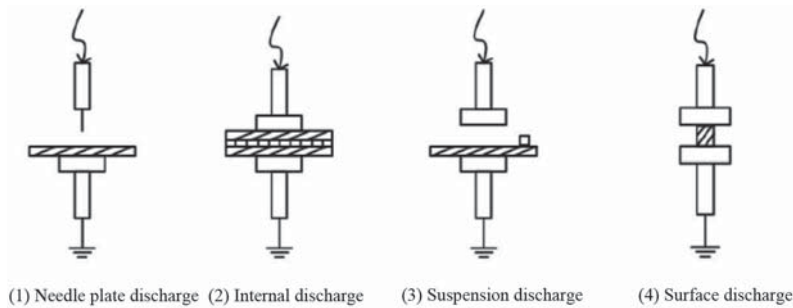
(1) Needle plate discharge (2) Internal discharge (3) Suspension discharge (4) Surface discharge
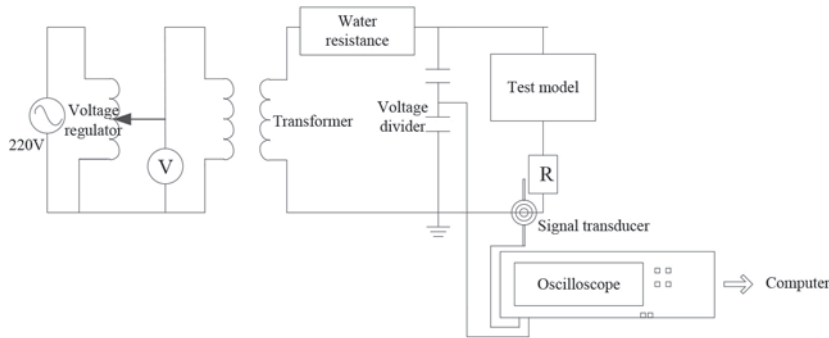
Figure 7 Four discharge types.

Figure 8 Experimental system device.

The electrodes of all the above-mentioned plates are round copper plates with a diameter of 50 mm and a thickness of 10 mm. In order to eliminate the influence of sharp corners or burrs on the electrode surface, the surface and edges of the electrodes are polished smooth. In order to prevent the electrode lead from discharging, the electrode has a a specially designed and processed spherical nut.

The insulation defect of cable joint interface is simulated to test the insulation discharge diagnosis of the cable end. The experiment was carried out in a high-voltage laboratory environment. The insulation level of the interface of the cable joint is relatively high, and the interface and electrode of the simulation are relatively small, so the discharge range is not large. Therefore, an accurate and simple test platform was needed. The circuit schematic diagram of this experiment is shown in Figure 8. The power-frequency voltage can generate high voltage and be applied to both ends of the test product by means of the voltage regulator, in which water resistance plays a protective role.

3.2 Results Analysis

For comparison with the method proposed in this paper, experiments are conducted using the reference [5] method and the reference [6] method. The diagnostic accuracy of each method is determined by comparing it with the diagnostic accuracy obtained by the other methods. The comparison results are shown in Figure 9.

For the needle plate discharge, the diagnostic accuracy of the reference [5] method ranges from 73% to 85%, that of the reference [6] method ranges from 66% to 83%, and the diagnostic accuracy of the method proposed in this paper ranges from 93% to 99%. For the internal discharge type,

the internal discharge diagnosis accuracy of the reference [5] method ranges from 73% to 85%, the internal discharge diagnosis accuracy of the reference [6] method ranges from 72% to 83%, and the internal discharge diagnosis accuracy of the method proposed in this paper ranges from 95% to 99%. For the suspended discharge type, the diagnostic accuracy of the reference [5] method ranges from 70% to 80%, that of the reference [6] method ranges from 77% to 81%, and diagnostic accuracy of the method proposed in this paper ranges from 95% to 98%. For the surface discharge type, of the accuracy of the reference [5] method ranges from 68% to 80%, that of the reference [6] method ranges from 68% to 81%, and the accuracy of the method proposed in this paper ranges from 97% to 99%. Of the three methods tested for comparison, the proposed method has the highest accuracy in terms of discharge diagnosis, and can achieve accurate diagnosis of the insulation discharge of high-voltage cable heads.

The diagnosis efficiency of each of the three methods (reference [5], reference [6] and the proposed method) was tested for comparison. The comparative efficiency was determined by comparing the diagnosis time required by each of the three methods. The results are shown in Tables 2–4.

In the data presented in Tables 2–4 show that the average diagnostic time of the reference [5] method is 1.44 s, the average diagnostic time of the reference [6] method is 2.30 s, and the average diagnostic time of the method proposed in this paper is 0.48 s; For the internal discharge type of insulation, the average diagnostic time of the reference [5] method is 1.75 s, the average diagnostic time of the reference [6] method is 2.04 s, and the average diagnostic time of this paper method is 0.49 s; For the suspension discharge type, the average diagnostic time of the reference [5] method is 1.01 s, the average diagnostic time of the reference [6] method is 3.46 s, and the average diagnostic time of the method proposed in
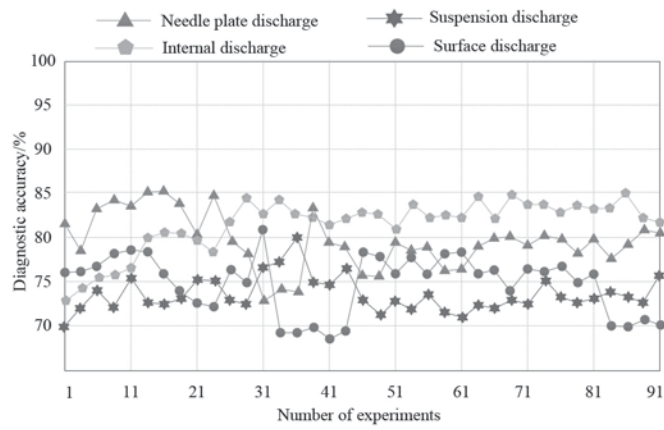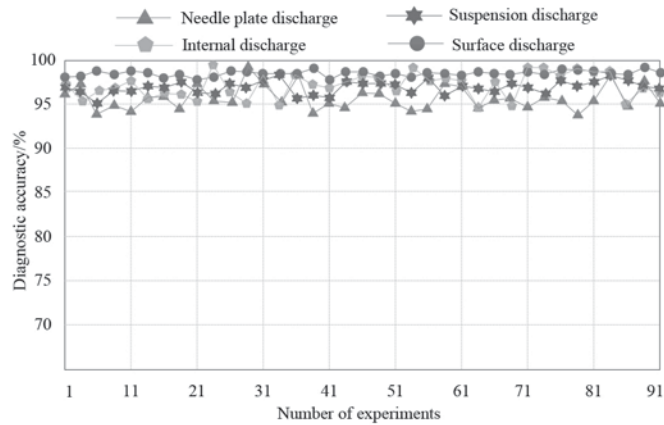
(a) Reference [5] method
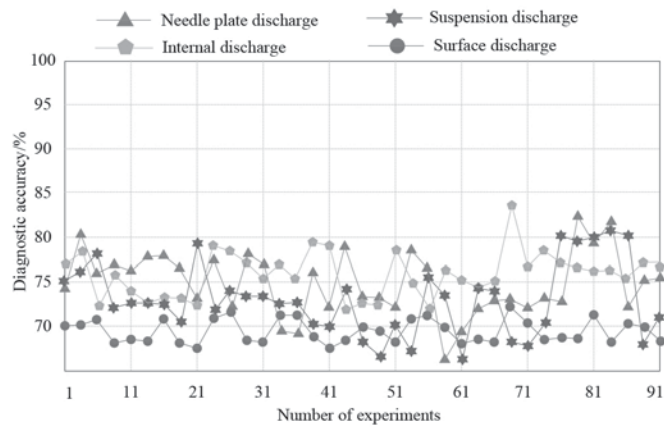
(b) Reference [6] method

(c) Paper method

Figure 9 Comparison of diagnostic accuracy of different methods.

this paper is 0.41 s; For the surface discharge type of high voltage cable head such as, the average diagnostic time of reference [5] method is 1.68 s, the average diagnostic time of reference [6] method is 2.36 s, and the average diagnostic time of the method proposed in this paper is 0.50 s. No matter what type of high voltage cable head insulation discharge, the fault diagnosis time of the proposed method is the shortest, which verifies that this method requires less diagnosis time and has greater diagnostic efficiency.

4.   CONCLUSION

Power systems require that power cables have good electrical and mechanical properties and can be easily installed. In order to transmit long-distance and high-capacity electric energy, cable joints account for the majority of the laying process. Therefore, the normal operation of cable joints in the power system is of great significance, which is related to the security of the power grid and the development of the social economy.

Table 2 Diagnostic time of reference [5] method (unit: %).

Number of experiments	Needle plate discharge	Internal discharge	Suspension discharge	Surface discharge
10	1.36	1.69	0.96	1.87
20	1.25	1.78	0.85	1.97
30	1.47	1.56	0.79	1.63
40	1.58	1.85	0.94	1.47
50	1.23	1.94	1.01	1.58
60	1.66	1.75	1.13	1.96
70	1.58	1.78	1.15	1.33
80	1.47	1.86	1.02	1.57
90	1.33	1.55	1.32	1.74
Average value	1.44	1.75	1.01	1.68

Table 3 Diagnostic time of reference [6] method (unit: %).

Number of experiments	Needle plate discharge	Internal discharge	Suspension discharge	Surface discharge
10	1.84	2.01	2.69	2.31
20	2.32	1.98	4.78	1.85
30	2.57	1.47	4.78	2.65
40	1.48	1.67	2.63	2.87
50	2.63	1.85	3.58	2.01
60	2.49	2.21	3.69	2.55
70	2.52	2.31	3.54	2.71
80	2.38	2.36	2.98	2.36
90	2.49	2.58	2.51	1.97
Average value	2.30	2.04	3.46	2.36

Table 4 Diagnostic time of the proposed method (unit: %).

Number of experiments	Needle plate discharge	Internal discharge	Suspension discharge	Surface discharge
10	0.52	0.47	0.39	0.69
20	0.36	0.38	0.35	0.57
30	0.41	0.46	0.41	0.58
40	0.45	0.39	0.36	0.45
50	0.46	0.54	0.57	0.47
60	0.38	0.51	0.52	0.41
70	0.56	0.49	0.45	0.39
80	0.58	0.61	0.36	0.47
90	0.61	0.58	0.29	0.46
average value	0.48	0.49	0.41	0.50

At present, there are many cable-related accidents. According to statistics, cable accidents occur mainly in the cable joint, because this structure is relatively complex compared with the cable body, and the insulation comprises a variety of materials. Cable joint failure will affect the normal operation of the whole system, and in serious cases will cause enormous economic losses and even casualties, both of which merit attention. Therefore, it is very important to have an effective diagnostic fault-detection method for high-voltage cable head insulation discharge. Hence, this paper proposes a diagnostic method based on multiple detection methods. The experimental results show that the diagnostic accuracy of needle plate discharge ranges from 93% to 99%, that of internal discharge ranges from 95% to 99%, that of suspended discharge ranges from 95% to 98%, and that of surface discharge ranges from 97% to 99%. The average needle plate discharge diagnosis time is 0.48 s, the average internal discharge diagnosis time is 0.49 s, the average suspended discharge diagnosis time is 0.41 s, and the average surface discharge diagnosis time is 0.50 s. This shows that the proposed method can achieve the important goal of rapid and accurate diagnosis of insulation discharge of high-voltage cable heads.

FUNDING

REFERENCES

1. Somsak T., Suwanasri T., Suwanasri C. (2021). Lifetime Estimation Based Health Index and Conditional Factor for Underground Cable System. *Energies, 14*(25):1–15.

2. Lelekhov S. (2021). Analysis of a possibility to use parallel non-twisted stacks of HTS tapes as cable in high current conductor of tokamak toroidal field coils. *IEEE Transactions on Applied Superconductivity, 31*(5):1–5.

3. Ovsyannikov E.A., Korolchenko D.A., Semikov VL. (2021). Extinguishment of cable fires at packaged transformer substations. *Pozharovzryvobezopasnost/Fire and Explosion Safety, 29*(6):84–90.

4. He Y., Lv Z., Wang X., et al. (2021). Comparison of Transportation Carriers in the Insulating Materials for HVDC Cable Joint. *IEEE Transactions on Dielectrics and Electrical Insulation, 28*(2):555–561.

5. Cao P., Xu Peng, Gao K., et al. (2020). Intelligent sensing and monitoring of cable joint operation state based on edge calculation. *High Voltage Apparatus, 56*(9):26–32.

6. Chen H., Xu Y., Qian S., et al. (2021). Distributed optical fiber ultrasonic sensor is used to detect the discharge fault of cable joint. *Acta Optica Sinica, 41*(3):22–30.

7. Pi H.S., Wei Y.S., Chen J.F. Partial discharge monitoring of cable joints based on optical fiber sensing technology. (2020). *Journal of Shenzhen University (Science and Engineering Edition), 37*(1):57–62.

8. Wu Z., He W., Zhang H., et al. (2021). Research on live detection technology of cable joint defects based on high-speed light sensing and pressure wave method. *Journal of Physics: Conference Series, 1871*(1):012015–012026.

9. Barbieri L., Villa A., Malgesini R., et al. (2021). An innovative sensor for cable joint monitoring and partial discharge localization. *Energies, 14*(14):1–12.

10. Li G., Wang Y., Xu X., et al. (2021). Intelligent cable joint quality management system based on RFID technology. *Journal of Physics: Conference Series, 1852*(2):022070–022077.

11. Zhang Y., Nie Y., Luo B., et al. (2021). Optimal design of functionally graded power cable joint utilizing silicone rubber/carbon nanotube composites. *IEEE Access, 99*:123689–123703.

12. Hr A., Ying Z.B. (2021). Analysis on switching overvoltage and suppression method of cable joint in 500 kV cable line. *Energy Reports, 7*(1):567–575.

13. Vu T., Teyssedre G., Roy S.L. (2021). Electric field distribution in HVDC cable joint in non-stationary conditions. *Energies, 14*(17):1–17.

14. Kim H., Park S., Yeo C., et al. (2021). Thermal analysis of 22.9-kV crosslinked polyethylene cable joint based on partial discharge using fiber Bragg grating sensors. *Optical Engineering, 60*(1):1–10.

15. Gao S., Jing Z., Chen H. (2021). A stable triple-wavelength semiconductor optical amplifier ring-cavity laser with two seed DFB lasers and a fiber Bragg grating. *Optik-International Journal for Light and Electron Optics, 238*(1):166725–166736.

16. Wang F., Wang B., Zhang X., et al. (2021). High sensitivity humidity detection based on functional GO/MWCNTs hybrid nano-materials coated titled fiber bragg grating. *Nanomaterials, 11*(5):1134–1149.

17. Qin Y., Wang Q., Xu D., et al. (2022). A fiber Bragg grating based earth and water pressures transducer with three-dimensional fused deposition modeling for soil mass. *Journal of Rock Mechanics and Geotechnical Engineering, 14*(2):663–669.

18. Ordin S. Introduction to Thermo-Photo-Electronics. *Journal of Eectronic & Information Systems*, 2023, 5(1):51–66.

19. Thamarai M., Aruna S.P., Sonti K., et al. Underwater Image Enhancement Using MIRNet. *Joumal of Eectronic & ifomation Systems*, 2023, 5(1):36–44.